RSC Advances

PAPER

View Article Online
View Journal | View Issue

Cite this: *RSC Adv.*, 2016, **6**, 33138

A copolymer capsule with a magnetic core for hydrophilic or hydrophobic drug delivery *via* thermo-responsive stimuli or carrier biodegradation†

Aihua Li,[ac] Hongjing Ma,[b] Shengyu Feng*[c] and Jingquan Liu*[ab]

In this work, we report the successful preparation of a dual-responsive polymer microcapsule carrier with a magnetic core, Fe_3O_4@capsule nanoparticles, by cross-linked polymerization of *N*-isopropylacrylamide and acrylamide in the presence of *N*,*N*′-bis(acryloyl)cystamine as a crosslinker. These novel drug carriers can undergo volume phase transition upon changing the environmental temperature or biodegradation of the polymer capsule by cleavage of the predesigned disulfide bonds within the crosslinker in the presence of glutathione (GSH) for hydrophilic or hydrophobic drug release. Herein, we take doxorubicin hydrochloride (DOX) as a hydrophilic drug model and curcumin as a hydrophobic drug model for investigating thermal responsiveness and biodegradation of magnetic polymer capsule carriers. Results indicate that DOX is released rapidly with thermal treatment and the release rate of DOX at PBS 5 is much faster than that at PBS 7.4. In addition, the release of water-insoluble drug curcumin is much faster with the assistance of GSH than without.

Received 28th December 2015
Accepted 20th March 2016

DOI: 10.1039/c5ra27839b

www.rsc.org/advances

1. Introduction

Polymer capsules have gained significant attention as a novel type of carrier for drug and gene delivery, owing to their unique properties including excellent biocompatibility, low toxicity, small size and large inner volume.[1–3] Besides, an important therapeutic index of nearly all drug delivery systems is that the drug molecules should be more efficiently delivered to the biological targets.[4] The best way to increase the efficacy and reduce the toxicity of any drug is to complete the transfer and control the release of drugs to its target at the right moment. To meet above requirements, a preferable drug delivery system should include the coordinating behavior of three components, the targeting moiety, the stimuli-responsive carrier, and the therapeutic drug. Therefore, a considerable effort has been devoted to the development of multifunctional polymer capsules. The common routes to direct drug carriers to "target" areas are reported to incorporate targeting molecules such as folic acid, peptide ligand[5] or magnetic nanoparticles[1,6] into polymer capsules.

In recent years, magnetic iron oxide, *e.g.*, Fe_3O_4 nanoparticles are of great interest as vehicles for drug delivery because they can guide drug molecules to the target organs or lesion sites inside the body. This helps in preventing the damage of normal organs or tissues due to drug toxicity before reaching the targeted location, thereby improving the therapeutic effect.[7] To be applied in biomedicine, the magnetic nanoparticles (MNPs) must have long term stability, small particle size, and magnetization as high as possible.[8] Apart from those properties, the MNPs have to be encapsulated by adding a coating on the surface of MNPs, which could prevent their aggregation in liquids and improve their chemical stability. In addition, to meet the second characteristic of the preferable drug delivery system, the stimuli-responsive polymeric carriers are usually designed with responsive moieties as the coating for Fe_3O_4 NPs which possess triggered release mechanisms to respond to intracellular stimuli, such as pH,[9] light,[10] temperature,[11] redox,[12,13] magnetic or electric properties,[14,15] *etc.* Among the previously reported stimuli responsive polymer, temperature responsive polymers are very popular.[4] One of the unique and exciting properties of thermal responsive polymers is the presence of a critical solution temperature (CST). These polymers can undergo structural and physical transitions with change in the environmental temperature. Below the lower critical solution temperature (LCST), the responsive polymer is

[a]*Shandong Provincial Key Laboratory of Detection Technology for Tumor Markers, College of Chemistry and Chemical Engineering, Linyi University Shuang Ling Road, Linyi, China. E-mail: jliu@qdu.edu.cn; Tel: +86-532-8378-0128*

[b]*College of Materials Science and Engineering, Qingdao University No. 308, Ning Xia Road, Qingdao, China. Tel: +86-532-8378-0128*

[c]*Key Laboratory of Special Functional Aggregated Materials and Key Laboratory of Colloid and Interface Chemistry (Shandong University), Ministry of Education, School of Chemistry and Chemical Engineering, Shandong University No. 27, South Shanda Road, Jinan, China. Tel: +86-531-8856-4464*

† Electronic supplementary information (ESI) available. See DOI: 10.1039/c5ra27839b

soluble in water and becomes insoluble, *i.e.*, formation of emulsion when above that.[16] Poly(*N*-isopropylacrylamide) (PNIPAM) is a well-known thermoresponsive polymer that exhibits the LCST of around 32 °C, which is slightly lower than body temperature. So several works have been reported to raise the LCST of PNIPAM by addition of acrylamide,[17,18] acrylic acid,[19] 2-carboxy isopropylacrylamide,[20] *etc.* as comonomer for controlled drug release in body.

Another key element for the preferable drug delivery system is therapeutic drug. A great number of temperature-responsive polymer systems were designed and synthesized to carry and control release of water-soluble drug molecules. Nevertheless, more than 40% of active compounds identified through screening of combinatorial libraries are poorly water-soluble, rendering them unsuitable for further drug development because of difficulties associated with their delivery using conventional formulation techniques.[2] Glutathione (GSH) exists in most cells as one of the most abundant reducing agents to balance the exchange reaction between thiol and disulfide, and subsequently manipulate the bioactivity.[12] The concentration of GSH in the cytosol was found to be about 1–11 mM. This specific property of GSH can be utilized to transfer water-insoluble drugs with controlled release at the right moment and in the right place.

Herein, we report a temperature-responsive polymeric nanocapsule with magnetic core as drug carrier for controlled drug release and carrier biodegradation (Scheme 1). First, Fe_3O_4 nanoparticles were prepared by hydrothermal method. Second, reversible addition–fragmentation chain transfer (RAFT) agent was anchored onto the surface of Fe_3O_4@SiO_2 microspheres. Finally, magnetic polymeric capsules were fabricated by cross-linked polymerization of NIPAM and acrylamide (AM) with magnetic RAFT agent, followed by the selective removal of silica template. Water-soluble drug molecules can be loaded into the hollow Fe_3O_4@capsule to achieve controlled drug release depending on the change of the environment temperature. For water-insoluble drug, we take curcumin as a model, which has been shown to suppress transformation, proliferation, and metastasis of tumors.[4] After encapsulation into the hollow cage of the magnetic polymer capsule, curcumin was gradually released along with biodegradation of thermal-responsive polymeric shell by redox between thiol group of GSH and disulfide bond of crosslinker.

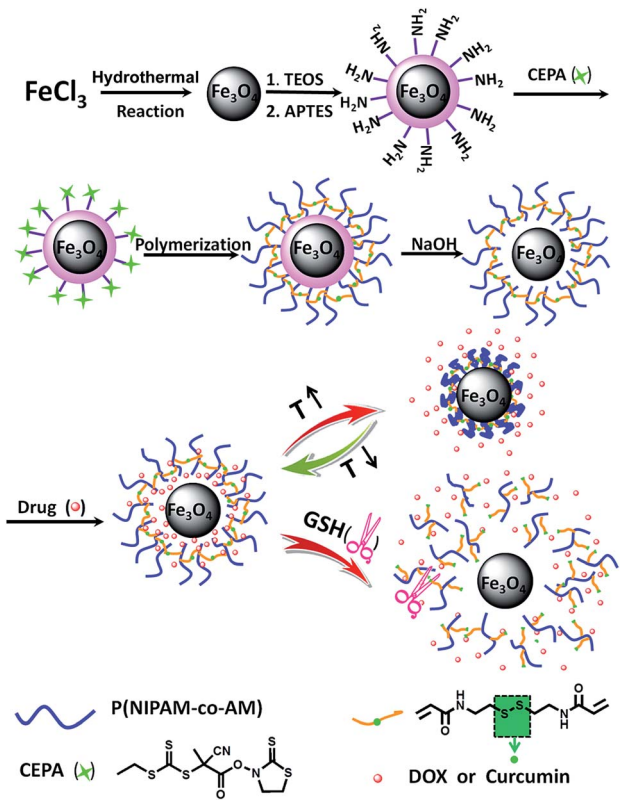

Scheme 1 Schematic illustration of the fabrication of dual-responsive P(NIPAM-*co*-AM) capsule with magnetic core and its stimuli-responsive mechanism.

2. Results and discussion

In this work, we designed and prepared dual-responsive polymeric capsule with magnetic Fe_3O_4 core for targeted drug delivery of hydrophilic anticancer drug, DOX and hydrophobic drug, curcumin. An illustration of the various steps involved in preparation of polymeric capsule coated magnetic Fe_3O_4 nanoparticles was given in Scheme 1. First, the magnetic NPs (Fe_3O_4) were produced by traditional hydrothermal method. The prepared Fe_3O_4 nanoparticles were then coated by silica *via* the well-known Stöber process, in which silica was formed *in situ* through the hydrolysis and condensation of TEOS, followed by grafting of 3-aminopropyl triethoxysilane (APTES). Further, the magnetic RAFT agent (Fe_3O_4@SiO_2–CEPA) was synthesized by a room temperature reaction between 4-cyano-4-ethyl-trithiopentanoic amide (CEPA) and Fe_3O_4@SiO_2–NH_2. Mercaptothiazoline ester of CEPA is a facile leaving group when attacked by the amine moiety to achieve amide coupling without destructing the RAFT active group, trithiocarbonate in a relatively neutral environment.[21,22] In addition, disulfide crosslinker *N*,*N*′-bis(acryloyl)cystamine was synthesized by amidation reaction between cystamine dihydrochloride and acryloyl chloride in the presence of triethylamine. Subsequently, NIPAM and AM monomers were copolymerized by RAFT polymerization using Fe_3O_4@SiO_2–CEPA as a macro-RAFT agent, AIBN as initiator, and *N*,*N*′-bis(acryloyl)cystamine as crosslinker, which resulted in the formation of Fe_3O_4@SiO_2@P(NIPAM-*co*-AM) composite microspheres with a core–shell structure. Finally, dual-responsive magnetic polymeric capsules, Fe_3O_4@P(NIPAM-*co*-AM), were obtained by immersing Fe_3O_4@SiO_2@P(NIPAM-*co*-AM) NPs into NaOH solution to removal of SiO_2 coating.

2.1. Characteristics of the prepared multifunctional Fe_3O_4@capsule NPs

The modification of the Fe_3O_4 NPs was monitored using XPS spectroscopy. XPS spectra of the bare Fe_3O_4 NPs indicated the existence of Fe and O (Fig. 1a). After modification with TEOS, APTES and CEPA, Fe_3O_4@SiO_2–CEPA was also characterized by

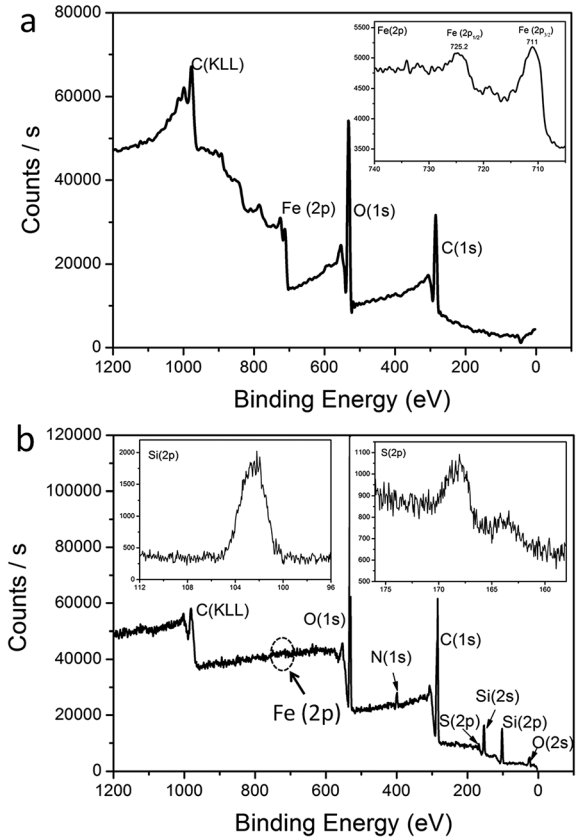

Fig. 1 XPS broad scan spectra: (a) Fe_3O_4 NPs and (b) Fe_3O_4/SiO_2–CEPA NPs. The insets are narrow scan spectra for Fe (2p), Si (2p) and S (2p).

XPS measurement as shown in Fig. 1b. From the narrow XPS scan spectrum of Fe (2p) in the inset of Fig. 1a, the peaks at 711.0 and 725.2 eV were the characteristic doublets of Fe ($2p_{3/2}$) and Fe ($2p_{1/2}$) from iron oxide. The data was consistent with the previous reported values of bare Fe_3O_4.[23] However, no characteristic peak for Fe was observed in curve of Fe_3O_4@SiO_2–CEPA NPs. The peaks at 103.6, 168.5 and 533.2 eV were assigned to Si (2p), S (2p) and O (1s), respectively. This indicated that SiO_2, APTES and CEPA were successfully deposited onto the Fe_3O_4 NP surface, forming the core–shell structure.

The surface charges of Fe_3O_4, Fe_3O_4@SiO_2, Fe_3O_4@SiO_2–NH_2 and Fe_3O_4@SiO_2–CEPA NPs were examined using ζ potential measurements in aqueous solution to obtain more insights on multifunctional magnetic NPs (Table 1). The bare Fe_3O_4 NPs showed a negative ζ potential of -29 ± 0.3 mV, indicating a negative charge on the surface of the Fe_3O_4 NPs. Fe_3O_4@SiO_2 NPs also exhibited a negative ζ potential of -13 ± 0.8 mV because of the presence of hydroxyl groups on the surface of SiO_2. Nevertheless, APTES modified Fe_3O_4@SiO_2 NPs showed a positive ζ potential of $+21 \pm 1.5$ mV due to the amine groups of APTES, which indicated APTES was successfully grafted onto the surface of Fe_3O_4@SiO_2 NPs. Fe_3O_4@SiO_2–CEPA nearly showed electric neutrality, revealing that neutral molecule, CEPA, had been anchored onto the surface of Fe_3O_4@SiO_2 by amidation.

Besides, the crosslinker *N*,*N*′-bis(acryloyl)cystamine was synthesized successfully by amidation of cystamine dihydrochloride with acryloyl chloride, as some new peaks were observed in the ^{1}H NMR spectrum as shown in Fig. 2a. For example, the peak signal at 6.55 ppm should be ascribed to the signal of the newly formed amide bond protons. The peak signals at 6.30 and 5.68 ppm represented the methylene protons from acryloyl chloride, which also indicated the successful reaction between cystamine dihydrochloride with acryloyl chloride. The peak signal at 6.21 ppm corresponded to the

Table 1 Values of the ζ potential of Fe_3O_4, Fe_3O_4@SiO_2, Fe_3O_4@SiO_2–NH_2 and Fe_3O_4@SiO_2–CEPA

Sample	Zeta(ζ) potential/mV
Fe_3O_4	-29 ± 0.3
Fe_3O_4@SiO_2	-13 ± 0.8
Fe_3O_4@SiO_2–NH_2	$+21 \pm 1.5$
Fe_3O_4@SiO_2–CEPA	-1 ± 1.2

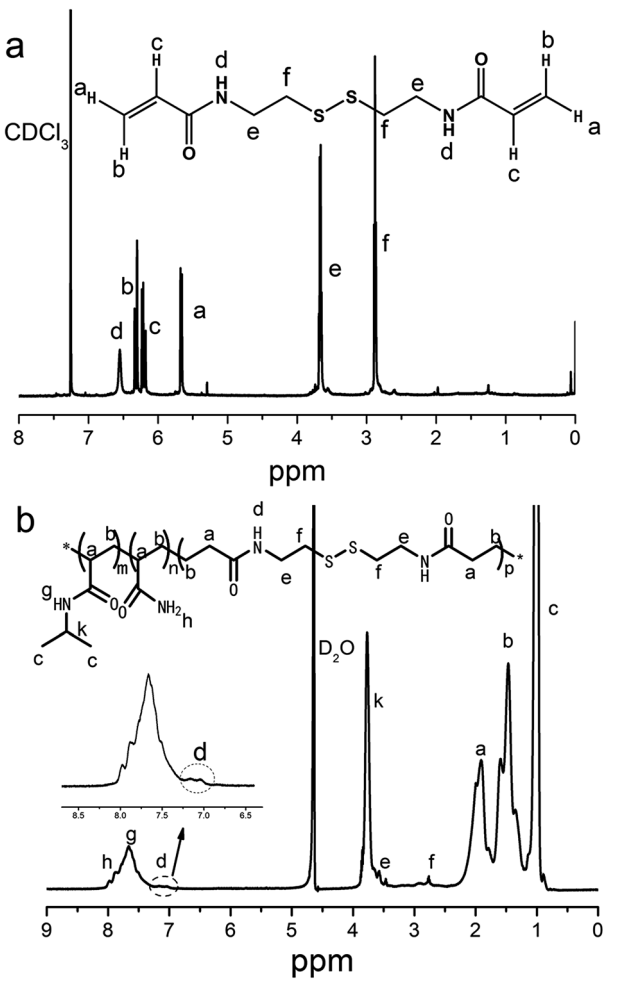

Fig. 2 ^{1}H NMR spectra: (a) crosslinker *N*,*N*′-bis(acryloyl)cystamine in $CDCl_3$ and (b) thermal polymer capsule after etching Fe_3O_4 NPs in D_2O (298 K, 600 MHz). The inset of (b) shows magnified peak signals of the protons from secondary amino of *N*,*N*′-bis(acryloyl)cystamine.

ethylene protons connected to carbonyl group. The peak signal at 3.67 ppm represented the methylene protons from cystamine dihydrochloride connected to amide group. The peak signal at 2.88 ppm indicated the presence of methylene protons next to the disulfide bond. The cross-linked polymer shell was prepared by RAFT polymerization with the monomers of NIPAM, AM and the synthesized crosslinker *N*,*N*′-bis(acryloyl)cystamine. The copolymer capsule was obtained by etching cross-linked polymer coated Fe_3O_4@SiO_2 NPs with hydrofluoric acid (HF) aqueous solution and characterized *via* ^{1}H NMR spectrum, as shown in Fig. 2b. The peak signals at 8.0 and 7.9 ppm corresponded to the protons from the amine group. The characteristic signals at 7.65 ppm represented the protons of secondary amine and that at 3.79 ppm from methine group both from PNIPAM portion. The peak signals at 3.55 and 2.85 ppm correspond to the protons of methylene group and the shoulder peak at 6.90–7.25 ppm corresponded to the secondary amine all from the crosslinker *N*,*N*′-bis(acryloyl)cystamine.

Representative transmission electron microscopy (TEM) images of magnetic Fe_3O_4 NPs, Fe_3O_4@SiO_2 NPs, Fe_3O_4@SiO_2@P(NIPAM-*co*-AM) NPs and P(NIPAM-*co*-AM) capsules with Fe_3O_4 cores were shown in Fig. 3. The Fe_3O_4 NPs were nearly sphere in shape, and had an average diameter of about 200 nm (Fig. 3a). The TEM image shown in Fig. 3b revealed that the core–shell structured magnetic silica microspheres possessed roughly 80 nm SiO_2 shells. Fig. 3c showed the TEM image of the double-shelled, spherical particles of Fe_3O_4@SiO_2@P(NIPAM-*co*-AM) NPs. The magnetic core was encapsulated in a gray silica layer, followed by coated with a bright P(NIPAM-*co*-AM) shell. In order to preserve the magnetic cores, the silica layer sandwiched between the magnetic core and the polymer shell has to be selectively removed. Usually, HF was selected to etch SiO_2. However, for this double-shelled magnetic composite, HF was not an appropriate etchant since Fe_3O_4 magnetic core could also been etched besides SiO_2 layer. Therefore, NaOH solution was chosen to etch the silica layers. The image of Fig. 3d showed that P(NIPAM-*co*-AM) capsule with a thickness of about 10 nm was left on the integrated magnetic core and SiO_2 layer disappeared subsequently. The removal of the SiO_2 layer afforded the well-defined hollow Fe_3O_4@P(NIPAM-*co*-AM) capsule for drug loading and controlled release. Furthermore, the size distribution of above four particles was also studied by dynamic light scattering (DLS) measurement (ESI, Fig. S1†). It was found that the PDI of synthesized magnetic Fe_3O_4 NPs was lowest compared to that of other three particles. The increase of PDI values for these three particles (Fe_3O_4@SiO_2 NPs, Fe_3O_4@SiO_2@P(NIPAM-*co*-AM) NPs and magnetic P(NIPAM-*co*-AM) capsules) may be attributed that some particles aggregated during the silica coating or polymerization process as manifested by the TEM images (Fig. 3).

The presence of surface functional groups on magnetic NPs was analyzed by FT-IR analysis. FT-IR spectra of bare Fe_3O_4 NPs, Fe_3O_4@SiO_2 NPs, P(NIPAM-*co*-AM) coated Fe_3O_4@SiO_2 NPs and

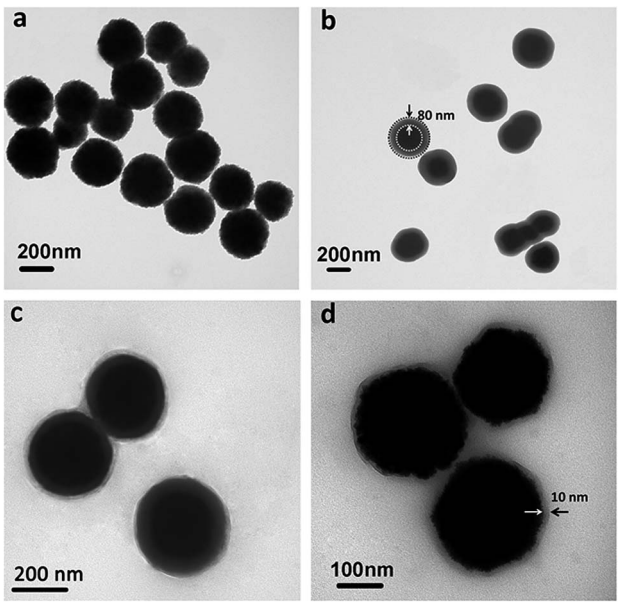

Fig. 3 TEM images: (a) bare Fe_3O_4 NPs, (b) Fe_3O_4@SiO_2 NPs, (c) Fe_3O_4@SiO_2@P(NIPAM-*co*-AM) NPs and (d) P(NIPAM-*co*-AM) capsules with Fe_3O_4 cores.

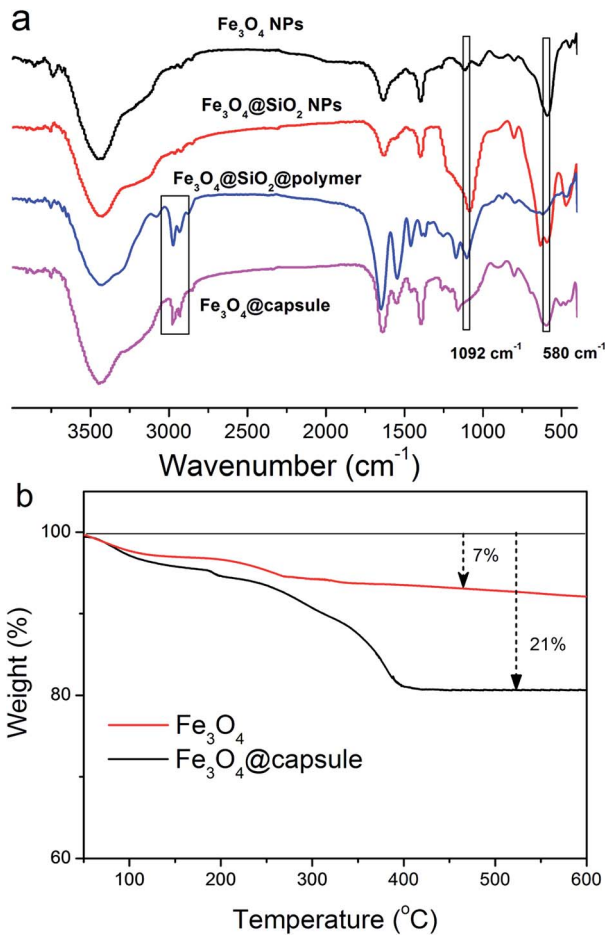

Fig. 4 (a) FT-IR spectra of bare Fe_3O_4 NPs, Fe_3O_4@SiO_2 NPs, Fe_3O_4@SiO_2@P(NIPAM-*co*-AM) NPs and P(NIPAM-*co*-AM) capsules with Fe_3O_4 cores, (b) TGA curves of Fe_3O_4 NPs and P(NIPAM-*co*-AM) capsules with Fe_3O_4 cores.

P(NIPAM-*co*-AM) capsules with Fe_3O_4 cores were shown in Fig. 4a. In the spectrum of Fe_3O_4, three main absorption peaks at 582, 1630 and 3380 cm^{-1} were observed, corresponding to Fe–O, O–H bending vibration and O–H stretching vibration, respectively. In the spectra of Fe_3O_4@SiO_2, a new peak at 1092 cm^{-1} appeared, corresponding to Si–O–Si bond stretching, which demonstrated the SiO_2 was successfully modified onto the surface of Fe_3O_4 NPs. After treatment with the copolymer, two bands for C–H stretching vibration of $-CH_3$ and $-CH_2$ of P(NIPAM-*co*-AM) appeared at 2930 and 2850 cm^{-1} respectively, suggesting successful polymer modification onto Fe_3O_4@SiO_2 NPs. For the spectrum of Fe_3O_4@P(NIPAM-*co*-AM) capsule, the characteristic peak of Si–O–Si stretching at 1092 cm^{-1} belonging to SiO_2 layer disappeared, indicating that SiO_2 was removed by NaOH solution and the P(NIPAM-*co*-AM) capsule with a magnetic core was prepared. The formation of the copolymer capsule encapsulated Fe_3O_4 nanoparticles was further corroborated by TGA measurements. It was observed from the TGA curves of bare Fe_3O_4 NPs and Fe_3O_4@P(NIPAM-*co*-AM) capsule that the curve of Fe_3O_4@capsule composite decreased significantly from 300 to 400 °C, which was consistent with the previous reported thermal degradation curve of copolymer P(NIPAM-*co*-AM),[18] while pure Fe_3O_4 NPs were fairly stable throughout the whole temperature range from 300 to 600 °C (Fig. 4b). In addition, it could be calculated from the TGA curves that the weight loss of Fe_3O_4 NPs and Fe_3O_4@capsule composite was 7 and 21 wt%, respectively. So the copolymer P(NIPAM-*co*-AM) cross-linked onto the surface of Fe_3O_4 NPs accounted for 14 wt% of the total mass of Fe_3O_4@capsule composite.

The temperature-induced dimensional changes of Fe_3O_4@P(NIPAM-*co*-AM) capsules were studied from 20 °C to 55 °C by DLS measurement. As shown in Fig. 5a, a dramatic phase transition took place around the LCST (about 40 °C) which was slightly above the normal temperature of the human body. At 20 °C, the hydrodynamic diameter of Fe_3O_4@P(NIPAM-*co*-AM) capsule was about 378 nm, which was much larger than that in the corresponding to TEM images, suggesting a good swelling performance of P(NIPAM-*co*-AM) polymer shell in aqueous media. After heated above 40 °C, the hydrodynamic diameter decreased rapidly to 240 nm, which was attributed to the volume phase transition of P(NIPAM-*co*-AM) capsule. In addition, the room temperature magnetization curves of Fe_3O_4 NPs and Fe_3O_4@P(NIPAM-*co*-AM) NPs are also measured as shown in Fig. 5b. It could be seen that the specific saturation magnetization (M_s) of P(NIPAM-*co*-AM) magnetic NPs was 31.10 emu g^{-1}, which was smaller than that of pure Fe_3O_4 (70.20 emu g^{-1}). The decrease in the value of M_s could be attributed to the coated polymer. However, the insets in Fig. 5b showed that the magnetic susceptibility of the resultant Fe_3O_4@P(NIPAM-*co*-AM) NPs was large enough to facilitate the quick separation of particles from solution using a regular magnetic plate in less than 20 s.

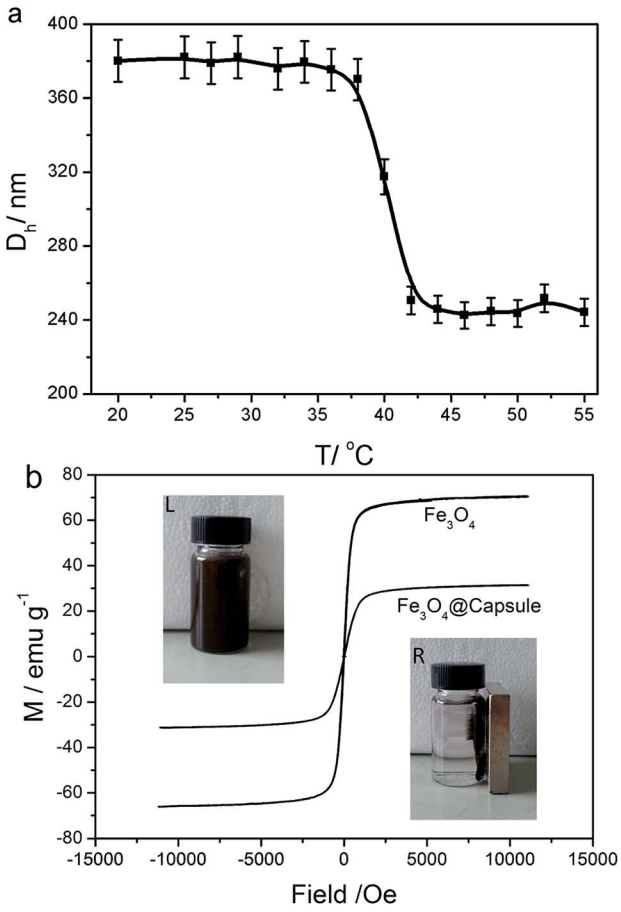

Fig. 5 (a) Hydrodynamic diameter of Fe_3O_4@P(NIPAM-*co*-AM) capsules as a function of temperature, (b) magnetic hysteresis loop of Fe_3O_4 NPs and Fe_3O_4@P(NIPAM-*co*-AM) NPs. The insets show the Fe_3O_4@P(NIPAM-*co*-AM) NPs dispersed in the water (L) and separation of Fe_3O_4@P(NIPAM-*co*-AM) NPs driven by a magnet (R).

2.2. *In vitro* drug loading and release study

The Fe_3O_4@P(NIPAM-*co*-AM) capsules were exposed to the drug solution, resulting in loaded drugs into the polymer shells *via* molecule diffusion. The Fe_3O_4@P(NIPAM-*co*-AM) capsules with higher drug loading could be obtained through increasing the mass ratio of drug to magnetic carriers. For instance, the loading capacity for DOX and curcumin could reach 18.35 and 19.64 wt% respectively, when the mass ratios of the drugs to particles were designed at 0.5. The diverse responsiveness to external stimuli of Fe_3O_4@P(NIPAM-*co*-AM) NPs provided an opportunity to fine-tune the release property of drug molecules.

The thermally tunable release of DOX. In view of the temperature-responsive property of P(NIPAM-*co*-AM) polymer capsule, the thermally triggered release of DOX was investigated. We prepared two phosphate buffer saline (PBS) solutions (pH 7.4 and 5) to simulate *in vivo* situations. The solution with pH 7.4 represents normal physiological conditions, whereas the intracellular pH value of general cancer cells environment is less than 5.5.[18,24] Two sets of Fe_3O_4@P(NIPAM-*co*-AM) NPs with equal amounts were prepared in PBS of pH 5 and PBS 7.4 with thermal treatment seven times as experimental groups (EGs), and the other two sets of such nanoparticles without thermal treatment but with the same time period were used as the control groups (CGs). At regular time intervals, thermal treated samples were taken out from the buffer solution by magnetic

separation and replaced with an equal volume of fresh buffer solution. The released amount of DOX was monitored by UV-vis spectrophotometry at its maximum absorption (480 nm) and calculated based on the UV absorption standard curve of free DOX (ESI, Fig. S2†). As shown in Fig. 6a, DOX release of experimental groups was faster than that of the control groups. This phenomenon was attributed to the rapid phase transition of P(NIPAM-*co*-AM) capsules from hydrophilic to collapsed (insoluble) state and the DOX buffer solution was dramatically extruded from the Fe_3O_4@P(NIPAM-*co*-AM) capsule carriers. Furthermore, it was observed that the release of DOX from magnetic carriers at pH 5 was faster, compared with that at pH 7.4 with the increasing time for both experimental and control groups. This may be due to the protonation of NH_2 on DOX under acidic conditions which was beneficial to the release of DOX. A similar phenomenon was also observed in other DOX-loaded particles or micelles.[13,25]

The thermally tunable release of DOX. The acid-sensitivity is also desirable for controlled drug release. GSH, which existed in most cells as one of the most abundant reducing agents to balance the exchange reaction between thiol and disulfide, was selected as reducing agent to cleave the disulfide bonds of crosslinker in P(NIPAM-*co*-AM) capsules, resulting in the biodegradation of polymer carrier and the release of water-insoluble drug (curcumin). In this work, to study GSH mediated reduction cleavage of disulfide bonds in cross-linked capsule and release of water-insoluble curcumin, the PBS solution (pH 7.4) containing 10% ethanol was selected. Because curcumin was soluble in ethanol, it was easily monitored by UV-vis spectrophotometer at its maximum absorption wavelength (427 nm) and the release amount could be calculated based on the UV absorption standard curve of curcumin in PBS solution containing 10% ethanol (ESI, Fig. S3†). In addition, in order to exclude the influence on free diffusion of curcumin from the polymer carriers, we also dispersed the same amount of magnetic carriers NPs into the mixed solvent without adding GSH reducing agent as a control. As shown in Fig. 6b, a larger amount of curcumin was released after adding GSH, compared to the sample without GSH. What's more, with the increase of the concentration of GSH, the release of curcumin became faster. As previously discussed, the addition of reducing reagent caused magnetic polymer carriers to dissociate into bare Fe_3O_4 NPs and linear copolymer. As a result, encapsulated curcumin was rapidly released as demonstrated by Fig. 6b. It was obviously that the redox-triggered release of curcumin was much higher than that *via* the free diffusion release process.

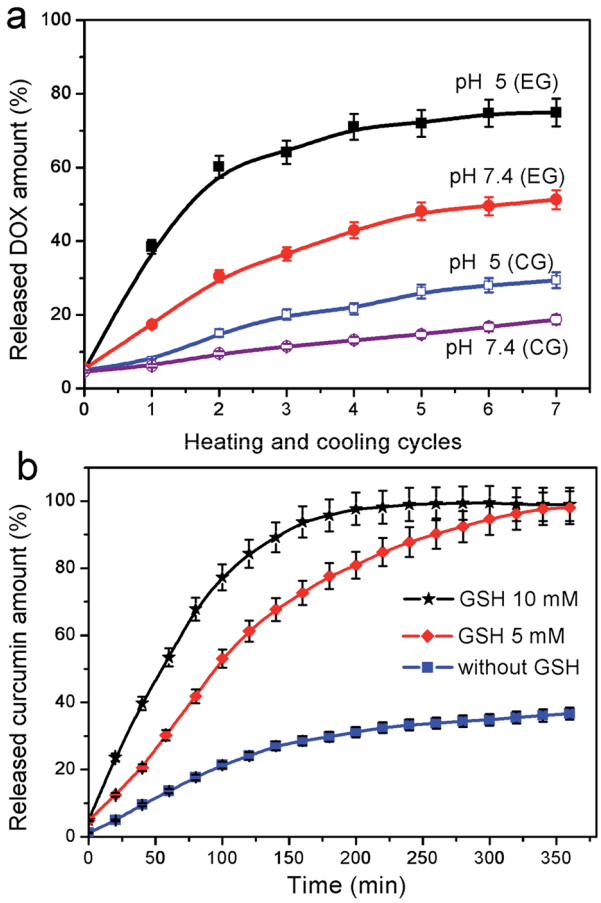

Fig. 6 (a) The cumulative release of DOX from the magnetic capsules in PBS at pH 7.4 and 5 with or without several thermal treatments. EG represents the experimental group with heating and cooling treatment, CG represents the control group without thermal treatment but at the same time period; (b) the redox-triggered release of curcumin in PBS solution (pH 7.4) containing 10% ethanol at 37 °C.

2.3. *In vitro* drug release study

In vitro cellular internalization of nanoparticles was analyzed by fluorescence microscopy. The human corneal keratocytes were incubated with DOX loaded Fe_3O_4@capsules and Fe_3O_4@capsules/curcumin, respectively for 12 h. Subsequently, the cells with Fe_3O_4@capsules/DOX were incubated at 42 and 37 °C repeatedly for several thermal treatment cycles. From Fig. 7a–d, the fluorescent images indicated the successful entry of NPs into cells through cytophagy. The weak red fluorescence shown in Fig. 7b before thermal treatment proved that only a small amount of DOX was released. However, after thermal treatment, the fluorescence was significantly enhanced, which demonstrated the release of DOX from the Fe_3O_4@capsule carriers was mainly dominated by thermal treatment. In addition, the cells with Fe_3O_4@capsule/curcumin were treated with GSH (50 μL, 10 mM). Due to the water-insolubility of curcumin, the curcumin was mainly encapsulated into the Fe_3O_4@capsule carriers, which resulted into many light spots as shown in Fig. 7f. However, after adding GSH, the curcumin was broadly diffused into the culture solution due to GSH mediated biodegradation of the capsule. As a result, the fluorescent spots became much darker as evidenced by Fig. 7h. In addition, in view of hydrophilic molecule DOX as the general anti-cancer drug, the release of DOX from Fe_3O_4@capsule/DOX NPs was also studied in cancer cells (HeLa cells) with several thermal treatments. As seen in Fig. 8b, the weak fluorescence was observed as well as some red spots, indicating that a large amount of DOX was still encapsulated in the Fe_3O_4@capsule carriers. However, with several thermal treatments, the strong fluorescence was seen and membrane shrinkage behavior was presented in Fig. 8d,

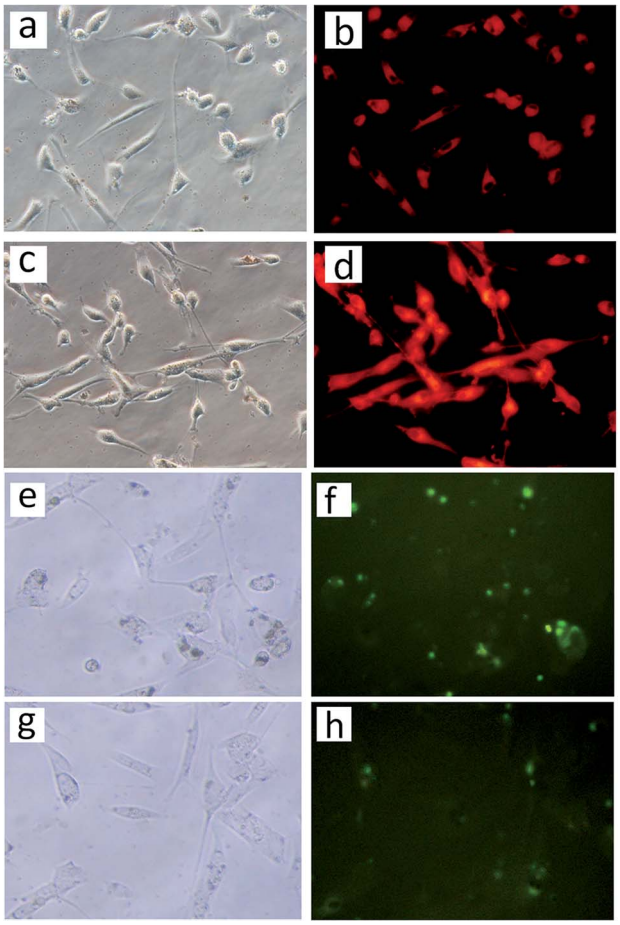

Fig. 7 Confocal microscopy images of the human corneal keratocytes. The images (a–d) were from the cells treated with Fe_3O_4@capsule/DOX (a, b) before and (c, d) after several thermal treatments. The images (e–h) were obtained from the cells treated with Fe_3O_4@capsule/curcumin (e, f) before and (g, h) after adding GSH. (a, c, e, g) are bright-field images; (b, d, f, h) are fluorescence images. The fluorescence signal (red) was from DOX and light-green from curcumin.

which may be attributed that DOX molecules were rapidly released resulting in the apoptosis of HeLa cells.

To achieve better application of Fe_3O_4@P(NIPAM-*co*-AM) capsule carriers in body, cell cytotoxicity was measured with the WST-8 assay, an approach which was widely used to quantify cell growth or cell death.[26] The cytotoxicity of synthesized magnetic capsules against normal cells (human corneal keratocytes) was evaluated as a function of the concentration of the NPs. It was observed from Fig. 9 that Fe_3O_4@P(NIPAM-*co*-AM) capsules showed no cytotoxicity on the corneal keratocytes at 0.1–100 μg mL^{-1} after incubation for 12 h and the cell viability were above 100%. However, when the concentration of magnetic capsule carriers reached 100 μg mL^{-1}, slightly reduced cell viabilities of 92% and 83% after incubation for 24 h and 48 h were observed, respectively. These results demonstrated that magnetic capsule carriers exhibited little toxicity to human cells at high concentration for long cultivation time.

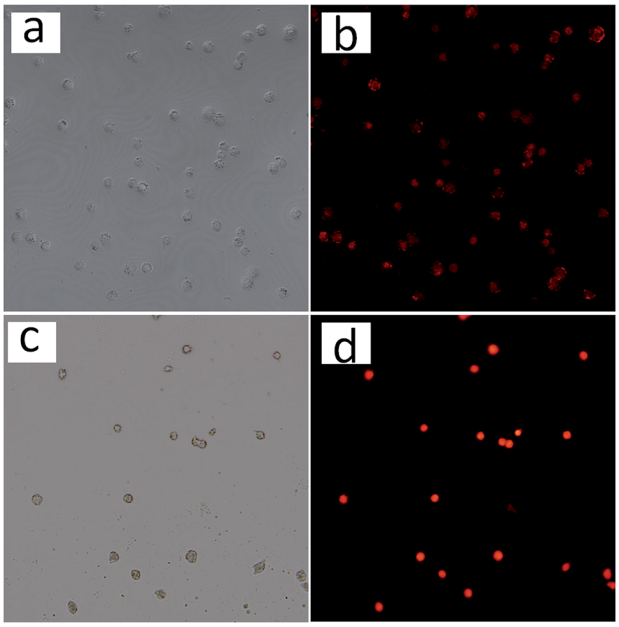

Fig. 8 Confocal microscopy images of HeLa cells treated with Fe_3O_4@capsule/DOX (a, b) before and (c, d) after several thermal treatments.

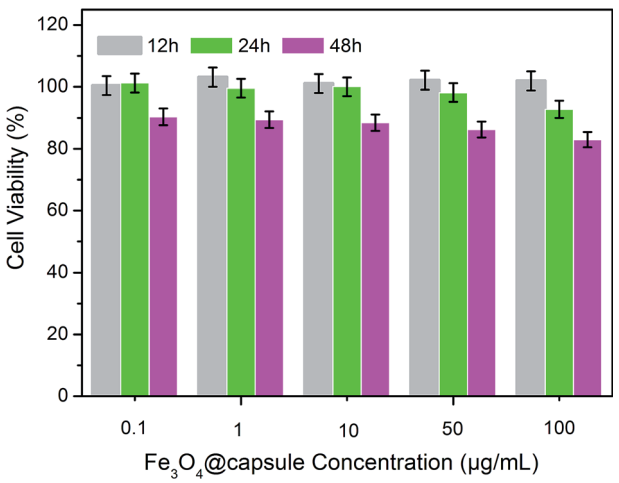

Fig. 9 Relative cell viabilities of human corneal keratocytes incubated with Fe_3O_4@P(NIPAM-*co*-AM) capsule carriers at different concentrations for 12 h, 24 h and 48 h.

3. Conclusions

In summary, dual responsive polymer capsule with magnetic Fe_3O_4 core was prepared by a facile method as drug carrier for hydrophilic or hydrophobic drug molecules. In the preparation process, the thermal-responsive polymer shell, P(NIPAM-*co*-AM) with LCST of 40 °C, was synthesized by RAFT polymerization and the silica sandwiched layer between the polymer shell and magnetic core was selected removed to obtain P(NIPAM-*co*-AM) capsule with Fe_3O_4 magnetic core. To investigate the drug loading property and controlled drug release, DOX and curcumin were used as hydrophilic and hydrophobic model drugs,

respectively. It was found that DOX could be released faster in PBS 5 than that in PBS 7.4 environment from these magnetic polymer capsules. In addition, the result showed that hydrophobic drug curcumin was gradually released in the presence of GSH *via* carrier biodegradation by reductive cleavage of the disulfide bonds in cross-linked capsules. From the MTT assay, it was demonstrated that the magnetic polymer capsule carriers were insignificantly cytotoxic at low concentration toward normal cells (human corneal keratocytes). The good biocompatibility, desired controlled drug release, and carrier biodegradation of the designed thermoresponsive magnetic capsule carrier set up the basis for future biomedical applications.

4. Experimental section

4.1. Materials

$FeCl_3 \cdot 6H_2O$, ethylene glycol, sodium acetate trihydrate (NaAc), trisodium citrate (Na_3Cit), concentrated ammonia aqueous solution ($NH_3 \cdot H_2O$, 28 wt%), hydrochloric acid (HCl), tetraethyl orthosilicate (TEOS), 3-aminopropyl triethoxysilane (APTES), triethylamine, acryloyl chloride, $NaHCO_3$, anhydrous Na_2SO_4, acrylamide (AM), azodiisobutyronitrile (AIBN) and NaOH were purchased from Tianjin Reagent Co., Ltd. *N*-Isopropylacrylamide (NIPAM), cystamine dihydrochloride, doxorubicin hydrochloride (DOX) and curcumin were purchased from Aladdin Reagent Co., Ltd (Shanghai, China). RAFT agent, 4-cyano-4-ethyl-trithiopentanoic amide (CEPA), was synthesized following previous published method.[22,27] All other reagents were of analytical grade and were used directly without further purification. Ultrapure water was obtained from a Nanopure Diamond, Barnstead purification system.

4.2. Preparation of Fe_3O_4 nanoparticles

Fe_3O_4 nanoparticles[28] were fabricated by hydrothermal treatment of $FeCl_3 \cdot 6H_2O$ and NaAc in ethylene glycol. In a typical procedure, 20 mmol of $FeCl_3 \cdot 6H_2O$ was dissolved in 40 mL of ethylene glycol to form a clear solution, followed by the addition of 40 mmol of anhydrous NaAc. The mixture was vigorously mixed by ultrasonication to give a homogeneous solution. Then the solution was transferred into a Teflon-lined stainless steel autoclave (50 mL capacity) for hydrothermal treatment at 200 °C for 10 h. After the autoclave was allowed to cool down to room temperature, the precipitate was collected by magnetic separation and washed several times under sonication with water and ethanol and then dried under vacuum at room temperature before characterization and application.

4.3. Preparation of CEPA modified Fe_3O_4@SiO_2 (Fe_3O_4@SiO_2–CEPA)

Fe_3O_4@SiO_2 microspheres were prepared according to the previously reported method.[29] Briefly, 0.10 g of Fe_3O_4 particles were homogeneously dispersed in the mixture of ethanol (80 mL), deionized water (20 mL) and $NH_3 \cdot H_2O$ (1.0 mL, 28 wt%), followed by the addition of TEOS (0.03 g, 0.144 mmol). After stirring at room temperature for 24 h, the Fe_3O_4@SiO_2 microspheres were separated by magnetic separation and washed with ethanol and water for three times, respectively. The obtained Fe_3O_4@SiO_2 magnetic particles were modified with excess APTES by stirring a mixture of silica dispersion and APTES (1 mL) for 12 h at room temperature in dry isopropanol (100 mL). The resulting APTES modified Fe_3O_4@SiO_2 (Fe_3O_4@SiO_2–NH_2) were collected by magnetic separation and washed several times with ethanol. Fe_3O_4@SiO_2–CEPA nanoparticles were prepared by re-dispersing the obtained Fe_3O_4@SiO_2–NH_2 nanoparticles in a solution of excess CEPA, CEPA (0.20 g, 0.55 mmol) in DMF (100 mL) and the resulting mixture was stirred at room temperature for 24 h. The expected product was collected by magnetic separation and washed several times with ethanol, followed by drying in a vacuum oven at 40 °C till constant weight.

4.4. Synthesis of crosslinker, *N*,*N*′-bis(acryloyl)cystamine

N,*N*′-Bis(acryloyl)cystamine was synthesized as the crosslinker for the preparation of responsive polymer capsule. In brief, cystamine dihydrochloride (1 g, 4 mmol) and triethylamine (1.5 mL) were dissolved in dry CH_2Cl_2 (30 mL), followed by the dropwise addition of acryloyl chloride (1 g, 11 mmol) in 20 mL dry CH_2Cl_2 at 0 °C in 2 h and then kept stirring for 12 h at room temperature. Then, distilled water (5 mL) was added into the mixture to dissolve the precipitate. The organic layer was washed with $NaHCO_3$ aqueous solution, dried over the anhydrous Na_2SO_4, and then concentrated under reduced pressure. The product was then dried under high vacuum for 12 h, and characterized by ^{1}H NMR as shown in Fig. 2a.

^{1}H NMR (600 MHz, $CDCl_3$) δ_H: 6.55 (s, 2H, –N*H*–C=O), 6.30, 5.68 (t, 4H, –CH_2=C), 6.21 (m, 2H, –C*H*–C=O), 3.67 (m, 4H, –CH_2–NH–), 2.88 (m, 4H, –S–CH_2–).

4.5. Preparation of P(NIPAM-*co*-AM) cross-linked copolymer coated Fe_3O_4 NPs

In the polymerization procedure, the Fe_3O_4@SiO_2–CEPA particles (25 mg) was used as macro-RAFT agent to control the polymerization of NIPAM (0.20 g, 1.76×10^{-3} mol), AM (14 mg, 1.97×10^{-4} mol) and *N*,*N*′-bis(acryloyl)cystamine (9.2 mg, 3.53×10^{-5} mol) in 100 mL DMF using AIBN (2 mg, 1.22×10^{-5} mol) as initiator. The reaction was allowed to proceed for 10 h at 75 °C under nitrogen atmosphere. Finally, the core–shell particles were collected by magnetic separation and washed with ethanol for three times.

4.6. Preparation of magnetic polymeric capsules, Fe_3O_4@capsule

The polymeric capsules were prepared by immersing the magnetic PNIPAM particles (0.1 g) in 2 M NaOH aqueous solution (10 mL) at room temperatures for 6 h. The resulting hollow magnetic capsules were collected by magnetic separation and washed several times with deionized water until pH 7.

4.7. Immobilization of drug molecules (*e.g.* DOX, curcumin) in magnetic polymeric capsules

5 mg of Fe_3O_4@capsule NPs was exposed to a solution of DOX (2 mL, 2 mg mL^{-1}) for 12 h, resulting in loading of the drugs into the magnetic capsules. The DOX-loaded micelles were collected by magnetic separation. The mass of DOX in the supernatant was determined by UV-vis spectrometry at 480 nm and calculated using the standard curve plotted by the absorbance at 480 nm *versus* the DOX concentration. The DOX loading efficiency was calculated using the following equation.

$$\text{Loading capacity} = \text{mass of drug loaded in the micelles/mass of micelles.}$$

Water-insoluble drug, curcumin was also loaded into Fe_3O_4@capsule NPs using similar strategy with PBS solution (pH = 7.4) containing 10% ethanol and the above formula applied to calculate loading efficiency of curcumin as well.

4.8. Drug molecules (DOX and curcumin) release study

DOX release from Fe_3O_4@capsule NPs. DOX loaded Fe_3O_4@capsule NPs were dispersed into two PBS buffers of pH values 5 and 7.4. Aliquots in two different PBS buffers were periodically treated with heating and cooling cycles (10 min each). Another two groups in the above solvents without the treatment of heating and cooling were used as blank controls. At pre-determined time intervals, samples (3 mL) were taken out from the buffer solution by magnetic separation and replaced with an equal volume of fresh buffer solution. The released amount of DOX can be easily monitored by UV-vis spectroscopy at 480 nm.

Curcumin release from Fe_3O_4@capsule NPs *via* carrier biodegradation. Reductively controlled release of curcumin in the Fe_3O_4@capsule NPs was evaluated by UV-vis absorption spectroscopy at different GSH concentration of 5 mM, 10 mM at 37 °C, respectively. A suspension of Fe_3O_4@capsule NPs (1 mg) in 3 mL PBS solution (pH = 7.4) containing ethanol (0.3 mL) and was bubbled with nitrogen for 30 min to remove the oxygen in case of GSH self-oxidation, followed by the addition of GSH (0.31 mg) and then stirred at 37 °C. At regular time interval (20 min), the supernatant (3 mL) was taken out by magnetic separation and amount of released curcumin was monitored by UV-vis absorption spectroscopy at 427 nm. The percentage of released curcumin was calculated from the calibration curve of free curcumin solution. Likewise, the curcumin releasing behavior was also studied at a GSH concentration of 10 mM at 37 °C. As a control, the release of curcumin was studied at 37 °C in the absence of GSH with the same condition.

4.9. Intracellular uptake of drug loaded Fe_3O_4@capsules and controlled release

The normal human corneal keratocytes (10^5 cells per sample) were plated onto 35 mm glass chamber slides. Fe_3O_4@capsule/DOX and Fe_3O_4@capsule/curcumin NPs were then freshly prepared and placed over the cells for 12 h at 37 °C with a 5% CO_2 atmosphere. Half of the corneal keratocytes incubated with above two drugs loaded magnetic nanoparticles were washed with PBS buffer three times at room temperature to remove the free NPs for fluorescence imaging using laser scanning confocal microscopy. The Fe_3O_4@capsule/DOX and Fe_3O_4@capsule/curcumin NPs were excited at 480 nm respectively. The cells with Fe_3O_4@capsule/DOX NPs was then incubated at 42 and 37 °C repeatedly for thermal treatments (30 min each), and the fluorescence images were taken correspondingly. In order to investigate the reductively controlled release of curcumin from the Fe_3O_4@capsule/curcumin NPs, the cells with Fe_3O_4@capsule/curcumin NPs were treated by adding GSH (50 μL, 5 mM) and incubated for another 4 h, followed by taking the fluorescence images.

As a general anti-cancer drug, doxorubicin release from magnetic copolymer capsule carriers was also performed into cancer cells (HeLa cells). HeLa cells (10^5 cells per well) were seeded into 6-well chambered coverglasses and cultured in fresh medium containing Fe_3O_4@capsule/DOX NPs at 37 °C under 5% CO_2. After 12 h incubation, half of the HeLa cells were washed with PBS buffer three times. The remaining half of HeLa cells with Fe_3O_4@capsule/DOX NPs were then incubated at 42 and 37 °C repeatedly for thermal treatments (30 min each), and the fluorescence images were taken correspondingly.

4.10. Cell cytotoxicity study of the Fe_3O_4@capsule carriers

The cell viability against the Fe_3O_4@capsule carriers was measured by MTT assay. Normal cells (human corneal keratocytes) were selected in 96-well plates with a density of 1×10^5 cells per mL and incubated with RPMI 1640 medium containing 10 v% fetal bovine serum at 37 °C under a humidified atmosphere with CO_2 (5%) for 24 h. Then, these cells were seeded with different concentrations of the synthesized Fe_3O_4@capsule NPs (0.1–100 μg mL^{-1}) for another 48 h. The absorbance was measured at 450 nm using a microplate reader (Bio-Rad). For the cell counting assay, cells were visualized under a microscope and manually counted. The cytotoxicity was expressed as the percentage of the cell viability relative to the blank control.

Acknowledgements

This work was funded by National Natural Science Foundation of China (51173087) for financial support.

Notes and references

1 J. Guo, W. Yang, Y. Deng, C. Wang and S. Fu, *Small*, 2005, **1**, 737–743.
2 Y. Wang, Y. Yan, J. Cui, L. Hosta-Rigau, J. K. Heath, E. C. Nice and F. Caruso, *Adv. Mater.*, 2010, **22**, 4293–4297.
3 A. Postma, Y. Yan, Y. Wang, A. N. Zelikin, E. Tjipto and F. Caruso, *Chem. Mater.*, 2009, **21**, 3042–3044.
4 S. Patra, E. Roy, P. Karfa, S. Kumar, R. Madhuri and P. K. Sharma, *ACS Appl. Mater. Interfaces*, 2015, **7**, 9235–9246.
5 A. Barhoumi, W. Wang, D. Zurakowski, R. S. Langer and D. S. Kohane, *Nano Lett.*, 2014, **14**, 3697–3701.

6 P. Du, B. Mu, Y. Wang, H. Shi, D. Xue and P. Liu, *Mater. Lett.*, 2011, **65**, 1579–1581.
7 B. Sahoo, K. S. P. Devi, R. Banerjee, T. K. Maiti, P. Pramanik and D. Dhara, *ACS Appl. Mater. Interfaces*, 2013, **5**, 3884–3893.
8 T. T. T. Mai, P. T. Ha, H. N. Pham, T. T. H. Le, H. L. Pham, T. B. H. Phan and X. P. Nguyen, *Adv. Nat. Sci.: Nanosci. Nanotechnol.*, 2012, **3**, 015006.
9 Y. Liu, W. Wang, J. Yang, C. Zhou and J. Sun, *Asian J. Pharm. Sci.*, 2013, **8**, 159–167.
10 D. He, X. He, K. Wang, Z. Zou, X. Yang and X. Li, *Langmuir*, 2014, **30**, 7182–7189.
11 C. Liu, J. Guo, W. Yang, J. Hu, C. Wang and S. Fu, *J. Mater. Chem.*, 2009, **19**, 4764–4770.
12 Z. Song, Y. Xu, W. Yang, L. Cui, J. Zhang and J. Liu, *Eur. Polym. J.*, 2015, **69**, 559–572.
13 X.-M. Zhang, K. Guo, L. H. Li, S. Zhang and B. J. Li, *J. Mater. Chem. B*, 2015, **3**, 6026–6031.
14 J. Wei, L. Ren, C. Tang and Z. Su, *Polym. Chem.*, 2014, **5**, 6480–6488.
15 J. Thévenot, H. Oliveira, O. Sandre and S. Lecommandoux, *Chem. Soc. Rev.*, 2013, **42**, 7099–7116.
16 D. Roy, W. L. Brooks and B. S. Sumerlin, *Chem. Soc. Rev.*, 2013, **42**, 7214–7243.
17 S. A. Shah, M. Asdi, M. Hashmi, M. Umar and S.-U. Awan, *Mater. Chem. Phys.*, 2012, **137**, 365–371.
18 A. Li, J. Zhang, Y. Xu, J. Liu and S. Feng, *Chem.–Eur. J.*, 2014, **20**, 12945–12953.
19 T. Saitoh, K. Asano and M. Hiraide, *J. Hazard. Mater.*, 2011, **185**, 1369–1373.
20 H. Wakamatsu, K. Yamamoto, A. Nakao and T. Aoyagi, *J. Magn. Magn. Mater.*, 2006, **302**, 327–333.
21 J. Liu, W. Yang, H. M. Zareie, J. J. Gooding and T. P. Davis, *Macromolecules*, 2009, **42**, 2931–2939.
22 X. Luo, J. Liu, G. Liu, R. Wang, Z. Liu and A. Li, *J. Polym. Sci., Part A: Polym. Chem.*, 2012, **50**, 2786–2793.
23 G. Du, Z. Liu, X. Xia, Q. Chu and S. Zhang, *J. Sol-Gel Sci. Technol.*, 2006, **39**, 285–291.
24 S. Zhang, Z. Chu, C. Yin, C. Zhang, G. Lin and Q. Li, *J. Am. Chem. Soc.*, 2013, **135**, 5709–5716.
25 X. Hu, X. Hao, Y. Wu, J. Zhang, X. Zhang, P. C. Wang, G. Zou and X.-J. Liang, *J. Mater. Chem. B*, 2013, **1**, 1109–1118.
26 J. H. Byeon and J. W. Kim, *ACS Macro Lett.*, 2014, **3**, 369–373.
27 J. Liu, E. Setijadi, Y. Liu, M. R. Whittaker, C. Boyer and T. P. Davis, *Aust. J. Chem.*, 2010, **63**, 1245–1250.
28 S. Liu, R. Xing, F. Lu, R. K. Rana and J. J. Zhu, *J. Phys. Chem. C*, 2009, **113**, 21042–21047.
29 J. Ge, Q. Zhang, T. Zhang and Y. Yin, *Angew. Chem.*, 2008, **120**, 9056–9060.